PCCP
Physical Chemistry Chemical Physics

Accepted Manuscript

This article can be cited before page numbers have been issued, to do this please use: J. P. K. Abal and M. C. Barbosa, *Phys. Chem. Chem. Phys.*, 2021, DOI: 10.1039/D1CP00613D.

ROYAL SOCIETY OF CHEMISTRY

rsc.li/pccp

View Article Online
DOI: 10.1039/D1CP00613D

PCCP

ARTICLE TYPE

Cite this: DOI: 00.0000/xxxxxxxxxx

Water mobility in MoS_2 nanopores: effects of the dipole-dipole interaction on the physics of fluid transport

João P. K. Abal[†,a], and Marcia C. Barbosa[†,b]

Received Date
Accepted Date

DOI: 00.0000/xxxxxxxxxx

Nanoscale materials are promising desalination technology. While fast water flow in nanotubes is well understood, this is not the case for water permeability in single-layer membranes. The advances in nanofluidics opened up the possibility to shift the permeability–selectivity tradeoff. The physical-chemical balance between nanopore size, shape, and charge might be the answer. In this work, we investigate the role of the MoS_2 nanopore charge distribution in water mobility by tuning its strength. We shed light on the competition between charge and nanopore size. The strong dipole interaction between water and the MoS_2 nanopore is responsible to append a constraint in the water angular orientation possibilities to travel through the nanopore, but this effect also depends on the nanopore size.

1 Introduction

A key challenge in the desalination process is creating a membrane where water is able to flow through and rejects salt ions. The most common process to separate salt from water is reverse osmosis, which consists of employing pressure to filter salt water. This process has two key parts: overcome the osmotic pressure and produce an efficient selective membrane. While the energy of overcoming the osmotic pressure has little space for improvement, the trade-off between selectivity and permeability represents the desalination process frontier[1]. The difficulty is that, in traditional polymeric membranes, a large enhancement in water permeability through increased pore size and permeability also implies an increase in salt permeability, which spoils selectivity. Therefore, a new physical phenomenon to increase water flow for small-sized pores was required[2–5].

This new phenomenon was the enhancement water flow inside nanoscale materials[6–8]. A number of studies have shown that sub-nanometer pores act as a highly selective and permeable filtration membrane with greater efficiency than current state-of-the-art polymer-based filtration membranes. The first system in which this property was observed was in carbon nanotubes (CNT). For diameters under 2nm[7,8], water molecules exhibit a flow five orders of magnitude larger than those observed in polymer-made membranes. The physical mechanism behind this enhanced mobility is the smooth inner hydrophobic surface of CNTs, which lubricates and speeds up a near-frictionless water transport[9]. The drawback is that hydrophobic carbon surfaces, even though not as frictionless for salt as it is for water, fail to repeal salt. Therefore, only CNTs with sub-0.9nm diameters are able to exhibit acceptable rejection rates[10]. In order to circumvent this problem, charged groups were added to the nanotube. The electrostatic forces added through the hydrophilic groups increased salt rejection, but decreased water velocity as well. Surface roughness produced by the hydrophilic groups also led to a reduction in water mobility[11]. Also, the hydrophilic substrate changes the behavior of water at least in layers very close to it[12]. Even though the physical mechanism behind the fast flow of water in CNTs is well understood, membranes based on it have been limited by low salt rejection rates and the difficulty of producing highly aligned and high-density CNT arrays.

The observations that the flux through membranes scales inversely with membrane thickness led to the idea of employing monolayer membranes as a new strategy for desalination. Posteriorly, several emerging classes of single-layer membranes have been proposed. Initially, exfoliated graphene as a single atomic layer membrane was proposed, followed by functionalized nanoporous graphene sheets[14–16] with several active groups and inorganic nanoparticles. The first attempt to investigate functionalized graphene for desalination demonstrated that functionalized nanoporous graphene membranes could perform more than 99% salt rejection and provide water permeance up to 2 or 3 orders of magnitude higher than that of current commercially available reverse osmosis membranes and nanofiltration membranes[14,17]. In addition, fast water flow through graphene nanocapillaries were also studied and the results indicate that the interaction with the hydrophobic confining walls induces structuring in water which significantly enhances the viscosity[18,19]. Since in the case of CNTs the frictionless flow in 2nm diameter pores explain the high permeability of water and the hydrophilic

‡Institute of Physics, Federal University of Rio Grande do Sul, 91501-970, Porto Alegre, Brazil
[a] joao.abal@ufrgs.br [b] marcia.barbosa@ufrgs.br

View Article Online
DOI: 10.1039/D1CP00613D

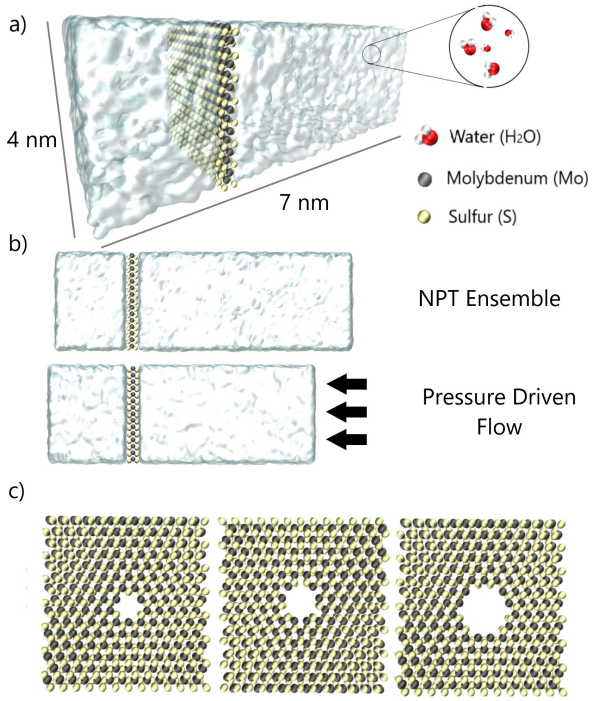

Fig. 1 (a) Simulation box with the MoS_2 nanoporous membrane, with water in both reservoirs and graphene layers as pistons applying pressure (images created using the Visual Molecular Dynamics software (VMD)[13]). **(b)** The illustration of the simulation steps: the NPT equilibration and the following pressure driven process. **(c)** The 0.74nm, 0.97nm, and 1.33nm nanopore diameters from left to right (considering the center-to-center distance of atoms).

functionalization, even though imposing additional friction helps rejecting salt, the mechanism and ingredients required for selectivity become clear. For atomic-sized pores, the concept of friction cannot be used. The selectivity observed in this case occurs for pores with one order of magnitude smaller than CNT pores. Therefore, although single-layer membranes seem to be the future for desalination, the physical-chemical reason for this enhancement flow is not clear. Besides that, there are many other 2D materials studied for water desalination applications, such as Boron Nitride Nanosheets[20], Covalent Organic Framework Nanosheets[21] and Metal–Organic Framework Membranes[22].

The physics behind fast water movement inside a single-layer pore might involve a number of effects usually irrelevant in larger systems: the dimensions inside the pore are comparable with the screening Debye length, which enhances electrostatic effects, and is also comparable with the unrestricted path between molecular collisions in water and with pore surface anisotropies[23]. In this context, many emerging classes of single-layer membranes have also been advanced, beginning with functionalized nanoporous graphene sheets[14,15,17]. Contrary to what happens in CNTs, water permeability for equal pore diameter is larger for hydrophilic groups than when compared with hydrophobic ones[14,15,17,24].

Water, a polar molecule, is naturally attracted to the charged hydrophilic pore surface. However, what is puzzling about this process is why the water molecules, once connected with the hydrophilic wall surface, move away from it in a higher velocity than that observed in a hydrophobic pore with the same pressure. The electrostatics of the system seem to play two competing roles: one to attract water to the pore, and another to repeal. These competing factors are enhanced in the case of the MoS_2 membrane[25–27]. This system has a higher water permeability than its equivalent graphene[26], mainly due to its lower water density near the membrane's surface, lower energy barrier to pass it and higher average water density and velocity inside the pore of MoS_2. The surprising effect is that this MoS_2 pore permeability is larger if the exposed atom at the pore is the divalent Mo when compared with the exposing monovalent S. Since pore sizes and shapes in both cases (Mo or S exposed) are slightly different, it is unclear if a larger exposed charge would enhance water velocity inside the pore, or if this larger velocity would be solely the result of its size and shape. Besides that, electrically controlled water permeation through graphene oxide membranes were experimentally studied and leads to the understanding that the ionization of water molecules inside graphene capillaries plays a crucial role in water transport, varying from fast flow to complete blocking[28].

2 Materials and Methods

In order to clarify these questions, we performed nonequilibrium molecular dynamic (NEMD) simulations for an MoS_2 membrane. In earlier attempts to answer to this question, the comparison was between graphene pores with charge-altering functionalization. The issue with this procedure was that, in order to alter the charge, the functionalization also changed the available pore area and shape. We created a simulation box full of interagent particles, as described in Figure 1(a), where two reservoirs of water molecules were separated by a MoS_2 nanoporous membrane. Through applying a pressure gradient in the box, the pressure-driven transport along the membrane initiates, as illustrated in Figure 1(b). This type of process helps us to get insights toward designing new membrane materials and to better understand the water-nanopore relationship.

	σ_{LJ} [Å]	ε_{LJ} [kcal/mol]	Charge (e)
O[29]	3.165	0.1848	-1.054
H[29]	0.0	0.0	0.5270
Mo	4.20	0.0135	0.0 ($q0$) / 0.6 ($q1$)[30] / 1.2 ($q2$)
S	3.13	0.4612	0.0 ($q0$) / -0.3 ($q1$)[30] / -0.6 ($q2$)
C[6]	3.40	0.0860	0.0

Table 1 The Lennard-Jones parameters and atoms charges employed in the simulations. The q_0 and q_2 charge parameters are fictitious.

To simply illustrate the complexity of tracking this problem, here we present the water permeability of an MoS_2 membrane under three conditions: a pore with no charge distribution (named q_0), a pore with Mo and S atoms with its normal charges (named q_1), and a pore with double the charge of Mo and S (named q_2). The first and last configurations are not physical, but they help

View Article Online
DOI: 10.1039/D1CP00613D

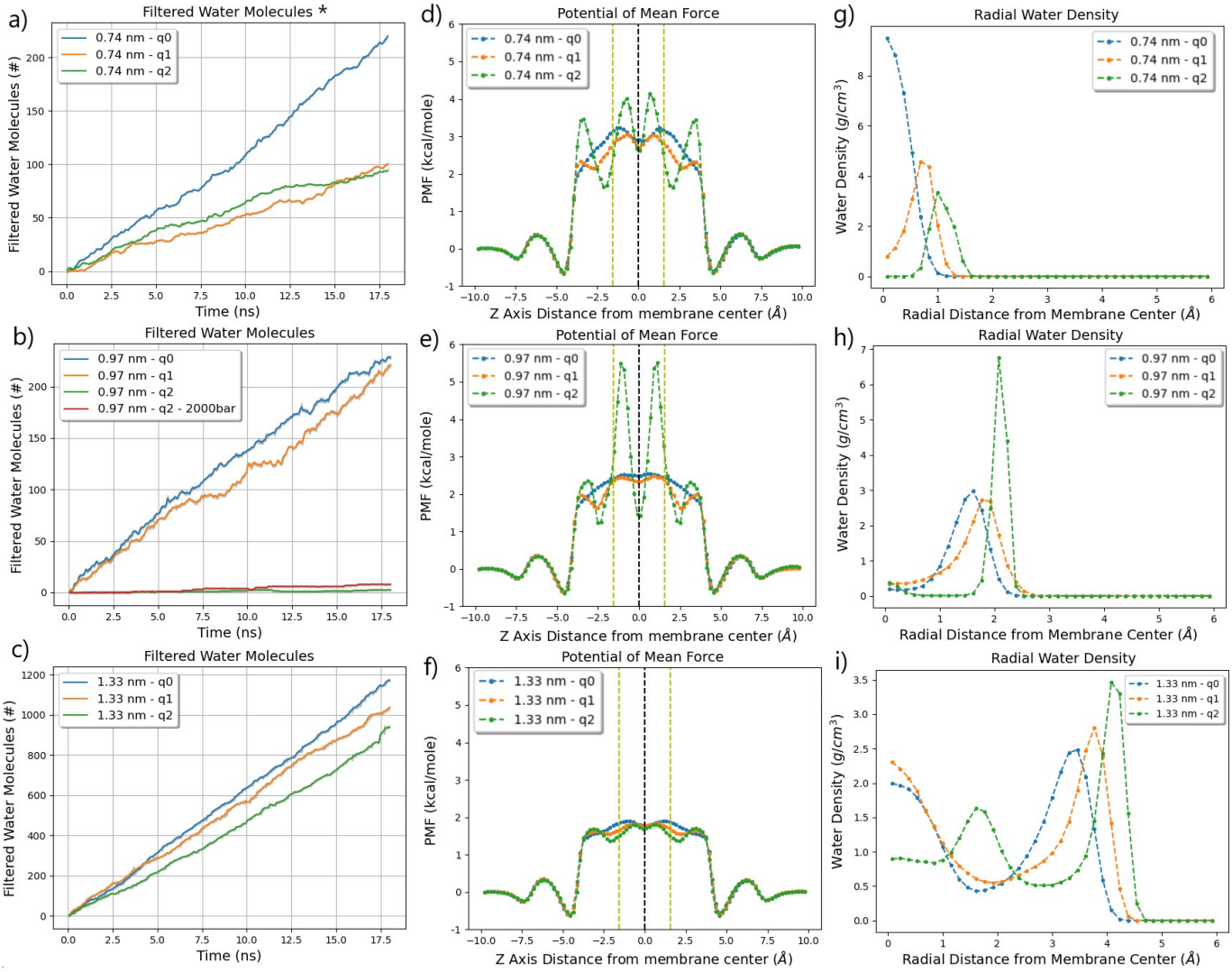

Fig. 2 (a-c) Filtered water molecules in function of time, (*) refers to a simulation with pressure gradient of 2000 bar for statistical purposes,**(d-f)** the potential of mean force (PMF) of water near and inside the nanopore (vertical dashed lines represent the Mo-black and S-yellow positions) and **(g-h)** radial water density inside the nanopore for each combination of size and charge values.

us to understand the role played by the charges in water mobility without changing pore size and shape, while also keeping intact the spacial distribution of the charge in the membrane.

In addition, three nanopore sizes were studied: 0.74nm, 0.97nm, and 1.33nm nanopore diameters (considering the center-to-center distance of atoms), as described in Figure 1(c). The NEMD simulations were performed using the Large-scale Atomic/Molecular Massively Parallel Simulator (LAMMPS) package[31]. We utilized the TIP4P/ε[29] water model and the parametrization of a reactive many-body potential as standard LJ parameters and charges values for Mo and S[30], as summarized in Table 1. The Lorentz-Berthelot mixing rules were used for non-bonded interactions. Long-range electrostatic interactions were calculated by the particle-particle-particle mesh method. We created a simulation box with 4nm x 4nm x 7nm, as illustrated in Figure 1-(a), with 3000 rigid water molecules. First, the particles were balanced during 2ns in an NPT ensemble in order to reach its $\approx 1\ g/cm^3$ equilibrium density at 300K and 1atm (Figure 1-(b)-top). Graphene pistons were used to control applied pressures. Afterwards, a 500 bar of pressure was imposed in the feed reservoir and the 18ns of non-equilibrium molecular dynamics (NEMD) running starts (Figure 1-(b)-bottom). Transported water molecules were collected on the other side of the membrane. The results were averaged over 3 different set of simulations.

3 Results

The water flowrate along MoS_2 illustrated in Figures 2(a)-(c) is affected by two competing factors: charge and size. In general, the uncharged system presents the fastest flow. We discussed the water mobility in terms of filtered water molecules because it is more useful to discuss the fluid transport for this size scale (< 2 nm of channel diameter) rather than viscosity or slip length, for example[32].

The charged pores, q_1 and q_2, form water clusters around Mo atoms, as shown in the color maps in Figure 3. In fact, the higher average water density around these sites were mentioned

View Article Online
DOI: 10.1039/D1CP00613D

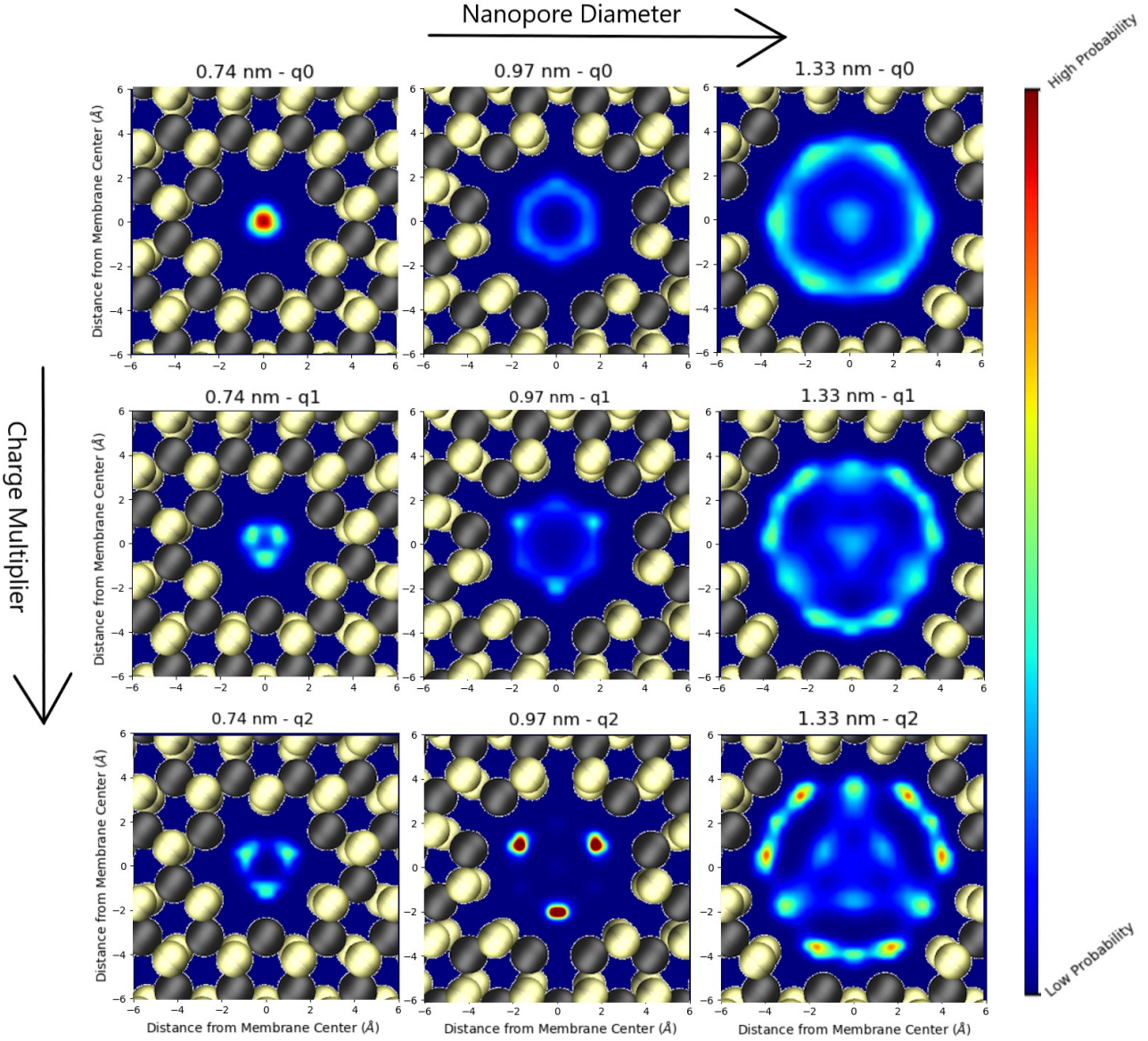

Fig. 3 Water flow density map (oxygen shown) for three different nanopore diameters and three different nanopore charge values. The illustration of the MoS_2 atoms doesn't represent the exact atoms positions.

before[26]. This behavior is similar to the observed functionalized carbon nanotubes[11], graphene nanopores[14,17] and $AlPO_4$-54 nanotubes[33], and it is dominated by electrostatics. However, for the 0.97nm pore something unexpected happens. The q_1 charge pore has practically the same mobility as the uncharged system ($\approx$ 4% less filtered water molecules). At this size, the electrostatic interaction attracting water to Mo and S is probably overcome by the hydrogen-bond network, which forces water to move apart from Mo and S. At this same size, but with q_2 charges, water gets stuck inside the nanopore (Figure 3) and the water flux stops Figures 2(b). Even at high-pressure levels (2000bar) the water molecules remain trapped in there.

The potential of mean force (PMF)[20,26,27] obtained from the local density $\rho(z)$, the bulk density ρ_0, the temperature T and Boltzmann constant k_b:

$$PMF(z) = -k_b T ln[\rho(z)/\rho_0] \,. \quad (1)$$

during the system equilibration procedure, illustrated in Figures 2(d)-(f) shows that for the q_2 case PMF has minima in Mo and near S sites. A small charge decrease from q_2 to q_1 flattens the PMF, which can only be understood if another force overcomes the electrostatic interactions and if water molecules move away from Mo and S as shown in the Figures 2(g)-(i). Also, from the PMFs shown in Figures 2(d)-(f) we can see the implications of tunning the nanopore charge are local with short range.

The PMFs in Figure 2(d)-(f) shows another interesting aspect of tuning the MoS_2 dipole strength without leaving it positive/negative charged: the effects are localized inside and near the nanopore. The implications are screened in the membrane interface and are not observed as registered by the PMF around

View Article Online
DOI: 10.1039/D1CP00613D

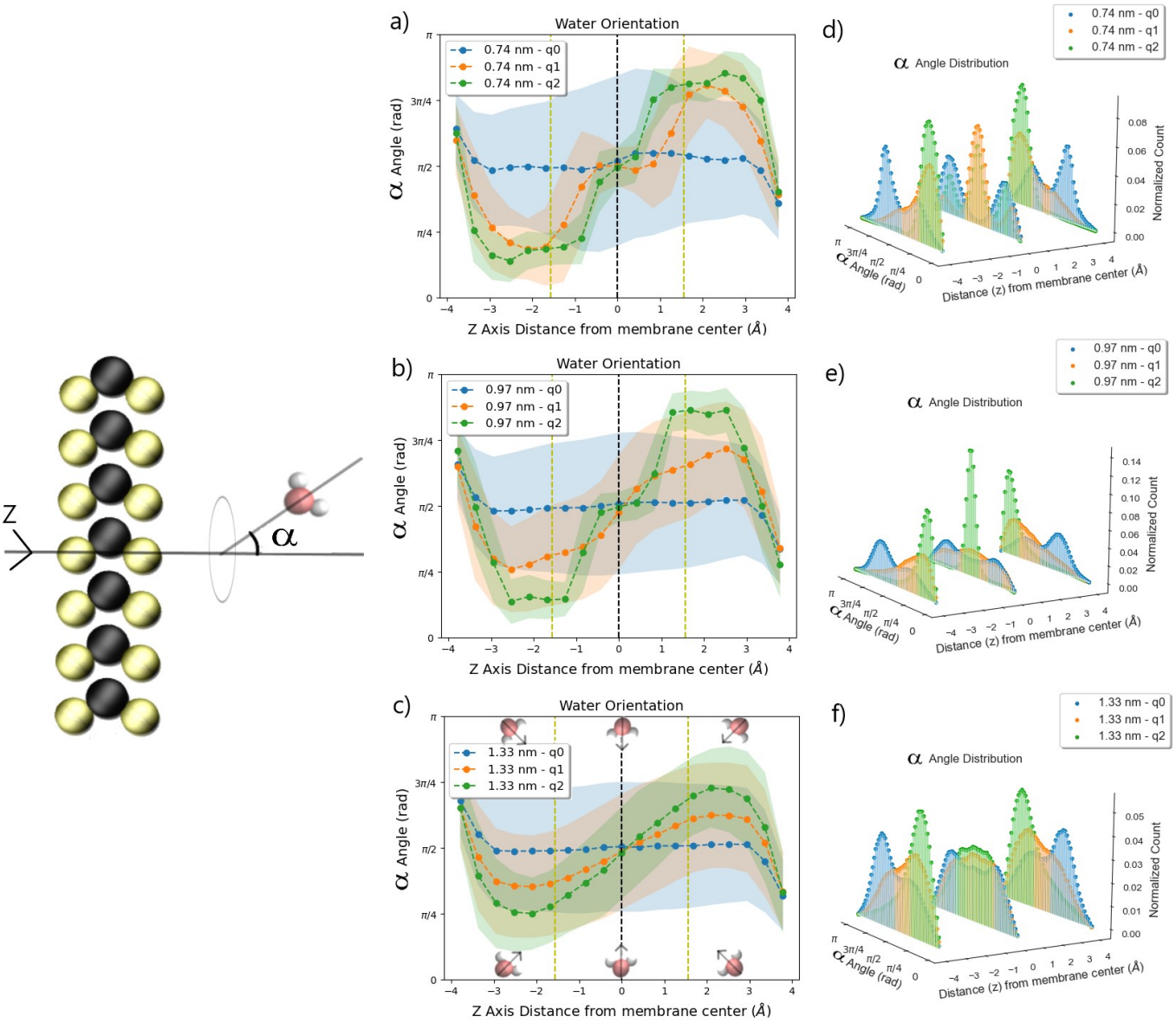

Fig. 4 (a-c) The water molecule orientation respect to the z axis as function of the membrane center distance. The colored shadow means one standard deviation attributed to each bin of analysis. The standard deviation was calculated taking into account different water molecules averaged in different simulations. **(d-f)** the α angle distribution inside the nanopore.

≈4 Å in the z-direction from the membrane center.

The differences between the water mobility through the 0.74nm and 0.97nm pore are intriguing. First it is interesting to note that the water flow map in the 0.74nm-q_0 is characterized by a single-file water molecules as observed in the radial water density map (Figure 2(g)), although the presence of charges split the single-file into three regions moving towards the Mo atoms. Besides that, as we can see from Figure 2(a), the presence of a charge distribution when the nanopore is too small, practically independent of its strength, is enough to slow down the water mobility but it is not enough to trap the water molecules there, in contrast with what happens in the Figure 2(b). The same phenomena can be seen from the density maps (Figure 3).

To clarify what happens with the water flux in the 0.74nm and 0.97nm pore, we conducted a series of angular analysis to better understand the entrance and exit effects of enhanced dipole interaction between water molecules and the tuned membrane. Figures 4(a)-(b) highlight the molecular rotation around and inside the nanopore. From that, it is clear the effects of q_2 and q_1 compared to the q_0 case: the charge distribution implies in dipole-dipole interaction which is responsible for limiting the possible angular configurations to pass through the pore. In contrast, the water molecules in the q_0 case are not so restricted in terms of assuming some specific angular state in order to pass through the pore (Figures 4(a)-(c)).

Figures 4(d)-(e) represent the evolution of the α angle distribution along the z axis. As we can see from it, the q_0 shows a range of angular possibilities and the rotation is not mandatory to pass through the pore while the q_2 and q_1 cases forces the molecule to rotate $\approx 90^\circ$ to be able to travel through the mem-

View Article Online
DOI: 10.1039/D1CP00613D

brane. The angular constraint surely impacts the water flow-rate. Sometimes, the constraint is so limited that the water molecules gets trapped inside the nanopore, as illustrated by Figure 3, Figure 2(b) and Figures 4(b)-(e) for the 0.97nm pore. In this case, the nanopore is larger so a higher number of water molecules fits in there. Attached to it, the hydrogen bond network is enhanced by the strong dipole interaction and contribute to the structure.

It is interesting to note from previous studies[11,14,15] that the ion selectivity is improved when the nanopore is functionalized. The functionalization procedure adds a charge distribution to the system and it improves the ion rejection by the membrane. As we can see from Figures 2(a)-(c), the addition of charges slow down the water flowrate in all nanopores sizes, but it is a well paid costs thinking in ion selectivity if the charge distribution is enough to allow practically the same water flux as observed by the comparison between q_0 and q_1 cases in Figures 2(b)-(c). In contrast, the cost is too high if the charge distribution can induce the nanopore blocking by strong water-MoS_2 dipole interaction, as illustrated in Figures 2(b)-(e)-(h).

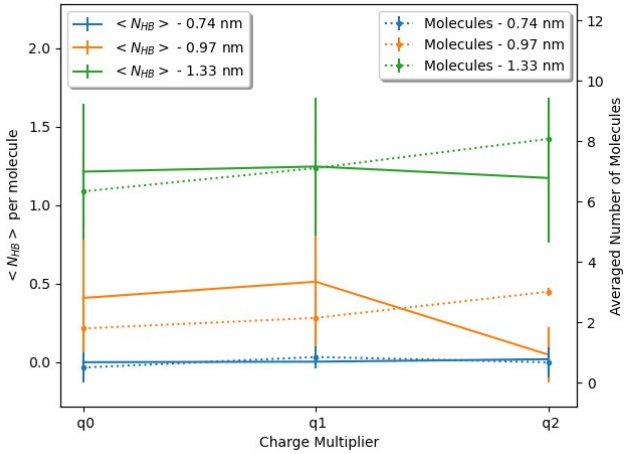

Fig. 5 Left axis) The averaged number of hydrogen bonds per molecule (N_{HB}) and **Right axis)** the averaged number of molecules inside the nanopore for each size and charge multiplier (q_0,q_1 and q_2). The N_{HB} was obtained considering distance criteria of $r_{O-O} < 3.5$ Å and angular criteria of $\theta_{OH-O} < 30°$ [34].

The water-MoS_2 dipole interaction and hydrogen bond network competition is the bridge mechanism that links the observed data. The narrow nanopore is so small that only one molecule in averaged fits in there, as illustrated by Figure 5. Furthermore, the 0.97nm nanopore fits 2 water molecules for the q_0 and q_1 systems, and the averaged number of hydrogen bonds per molecule (N_{HB}) is 0.5, but this is not true for the q_2 system. The 0.97nm with q_2 produce such high water-MoS_2 dipole interaction that makes it possible to fits 3 water molecules in there breaking the possibles N_{HB}. In this case, the water molecules assume an arrangement of position (see Figure 3) and angular orientation (see Figure 4(b)-(e)) that it gets trapped in there, with each water oxygen stuck in the nanopore edge (Mo sites) and with each hydrogen orientated to the center of the nanopore, producing zero N_{HB}. In this case, even high-pressure levels (2000bar) are not enough to push the water molecules through the 0.97nm pore (see Figure 2(b)). This competition explains the larger free energy barrier observed in the 0.97nm with q_2 system (see the PMF in Figure 2(e)). Then, comparing the 0.97nm/q_2 with the 0.74nm/q_2 case, it is possible to conclude that it is easier to push 1 molecule through the 0.74nm pore than 3 binding molecules through the 0.97nm pore. Besides, the 1.33nm nanopore has 6-8 water molecules inside and this makes it possible to maintain a hydrogen bond network strong enough to produce water flow even with q_2.

4 Conclusions

The mechanism for high water mobility inside nanopores involve the competition between local electrostatic forces and the cooperation of the hydrogen bond network. The strong dipole interaction is responsible to append a constraint in the the water angular orientation possibilities to travel through the nanopore, but this implication also depends on the nanopore size. As it was observed for the 0.97nm case, if the water-MoS2 dipole interaction is strong enough and the nanopore has the right geometry, the water molecules don't participate in the hydrogen bond network and get trapped inside the nanopore. This is the new trade-off in thinking about design the next-generation of nanoporous membrane materials. The pore size and charge surely impacts membrane permeability performance by different flow mechanisms. These nanopores needs a charge distribution in order to enhance the ion rejection, but not too much charge to trap water molecules into there depending on the nanopore size.

Acknowledgement

This work was supported by the Brazilian agencies CNPq (through INCT-Fcx) and Coordenação de Aperfeiçoamento de Pessoal de Nível Superior (CAPES). The authors thank the computational infrastructure from CENAPAD/SP and CESUP/UFRGS.

Conflicts of interest

The authors declare that they have no known competing financial interests or personal relationships that could have appeared to influence the work reported in this paper.

Notes and references

1 H. B. Park, J. Kamcev, L. M. Robeson, M. Elimelech and B. D. Freeman, *Science*, 2017, **356**, 356.
2 N. Voutchkov, *Desalination*, 2018, **431**, 2 – 14.
3 P. J. J. Alvarez, C. K. Chan, M. Elimelech, N. J. Halas and D. Villagrán, *Nature Nanotechnology*, 2018, **13**, 634–641.
4 J. R. Werber, C. O. Osuji and M. Elimelech, *Nature Reviews Materials*, 2016, **1**, 16018.
5 C. Fritzmann, J. Löwenberg, T. Wintgens and T. Melin, *Desalination*, 2007, **216**, 1–76.
6 G. Hummer, J. C. Rasiah and J. P. Nowryta, *Nature*, 2001, **414**, 188–190.
7 M. Majumder, N. Chopra, R. Andrews and B. J. Hinds, *Nature*, 2005, **438**, 44.
8 J. K. Holt, H. G. Park, Y. Wang, M. Stadermann, A. B.

View Article Online
DOI: 10.1039/D1CP00613D

Artyukhin, C. P. Grigoropoulos, N. A. and O. Bakajin, *Science*, 2006, **312**, 1034–1037.

9 A. Kalra, S. Garde and G. Hummer, *Proc. of National Acad. Sciences*, 2002, **100**, 210175–10180.

10 C. Song and B. Corry, *J. Phys. Chem. B*, 2009, **113**, 7662–7649.

11 Y. Hong, J. Zhang, C. Zhu, X. C. Zeng and J. S. Francisco, *J. Mater. Chem. A*, 2019, **7**, 3583–3591.

12 M. De Marzio, G. Camisasca, M. M. Conde, M. Rovere and P. Gallo, *The Journal of Chemical Physics*, 2017, **146**, 084505.

13 W. Humphrey, A. Dalke and K. Schulten, *Journal of Molecular Graphics*, 1996, **14**, 33–38.

14 D. Cohen-Tanugi and J. C. Grossman, *Nano Lett.*, 2012, **12**, 3602–3608.

15 D. Konatham, J. Yu, T. A. Ho and A. Striolo, *Lamgmuir*, 2013, **29**, 11884–11897.

16 C. T. Nguyen and A. Beskok, *Phys. Chem. Chem. Phys.*, 2019, **21**, 9483–9494.

17 Y. Wang, Z. He, K. M. Gupta, Q. Shi and R. Lu, *Carbon*, 2017, **12**, 120–127.

18 B. Radha, A. Esfandiar, F. C. Wang, A. P. Rooney, K. Gopinadhan, A. Keerthi, A. Mishchenko, A. Janardanan, P. Blake, L. Fumagalli, M. Lozada-Hidalgo, S. Garaj, S. J. Haigh, I. V. Grigorieva, H. A. Wu and A. K. Geim, *Nature*, 2016, **538**, 222–225.

19 M. Neek-Amal, A. Lohrasebi, M. Mousaei, F. Shayeganfar, B. Radha and F. M. Peeters, *Applied Physics Letters*, 2018, **113**, 083101.

20 H. Gao, Q. Shi, D. Rao, Y. Zhang, J. Su, Y. Liu, Y. Wang, K. Deng and R. Lu, *The Journal of Physical Chemistry C*, 2017, **121**, 22105–22113.

21 W. Zhou, M. Wei, X. Zhang, F. Xu and Y. Wang, *ACS Applied Materials & Interfaces*, 2019, **11**, 16847–16854.

22 Z. Cao, V. Liu and A. Barati Farimani, *Nano Letters*, 2019, **19**, 8638–8643.

23 L. Wang, M. S. H. Boutilier, P. R. Kidambi, D. Jang, N. G. Hadjiconstantinou and R. Karnik, *Nature Nanotechnology*, 2017, **12**, 509–522.

24 R. Jafarzadeh, J. Azamat and H. Erfan-Niya, *Estrutural Chemistry*, 2020, **31**, 293–303.

25 M. Heiranina, A. B. Farimani and N. R. Aluru, *Nature Communications*, 2015, **6**, 8616–8622.

26 Z. Cao, V. Liu and A. Barati Farimani, *ACS Energy Letters*, 2020, **5**, 2217–2222.

27 C. Liu, Y. Jin and Z. Li, *Journal of Applied Physics*, 2019, **126**, 024901.

28 K.-G. Zhou, K. S. Vasu, C. T. Cherian, M. Neek-Amal, J. C. Zhang, H. Ghorbanfekr-Kalashami, K. Huang, O. P. Marshall, V. G. Kravets, J. Abraham, Y. Su, A. N. Grigorenko, A. Pratt, A. K. Geim, F. M. Peeters, K. S. Novoselov and R. R. Nair, *Nature*, 2018, **559**, 236–240.

29 R. Fuentes-Azcatl and M. C. Barbosa, *Physica A: Statistical Mechanics and its Applications*, 2016, **444**, 86 – 94.

30 E. S. Kadantsev and P. Hawrylak, *Solid State Communications*, 2012, **152**, 909 – 913.

31 S. Plimpton, *Journal of Computational Physics*, 1995, **117**, 1 – 19.

32 S. K. Kannam, P. J. Daivis and B. Todd, *MRS Bulletin*, 2017, **42**, 283–288.

33 C. Gavazzoni, N. Giovambattista, P. A. Netz and M. C. Barbosa, *The Journal of Chemical Physics*, 2017, **146**, 234509.

34 J. Liu, X. He, J. Z. H. Zhang and L.-W. Qi, *Chem. Sci.*, 2018, **9**, 2065–2073.